Nonlinear strain theory of plastic flow in solids

Nonlinear strain theory of plastic flow in solids

Akira Onuki

Department of Physics, Kyoto University, Kyoto 606-8502, Japan

Abstract

We present a phenomenological time-dependent Ginzburg–Landau theory of nonlinear plastic deformations in solids. Because the problem is very complex, we first give models in one and two dimensions without vacancies and interstitials, where large strains produce densely distributed slips but the mass density deviations remain small except near the tips of slips. Next we set up a two-dimensional model including a vacancy field (or local free-volume fraction), where the sensitive dependence of the elastic shear modulus on the vacancy density is relevant. In our simulation, if strains are applied to nearly defectless solids but in the presence of such an elastic inhomogeneity, the vacancy density and the mass density can become considerably heterogeneous for large strains on spatial scales much longer than the atomic size. These strain-induced disordered states are metastable or long lived once they are created.

1. Introduction

Most previous papers on glass transitions so far have been concerned with near-equilibrium properties such as relaxations of the density time correlation functions or dielectric response. However, these quantities are too restricted or indirect, and there remains a rich group of unexplored problems in far-from-equilibrium states. In particular, shear is a relevant perturbation drastically changing the glassy dynamics when the shear rate $\dot\gamma$ exceeds the inverse of the structural relaxation time τ_α [1, 2]. In supercooled liquids, the microscopic rearrangement processes occur on the timescale of τ_α in quiescent states, whereas they are much accelerated even by extremely small $\dot\gamma$ (if larger than τ_α^{-1}). Similar *jamming rheology* has been studied in systems composed of large elements such as colloidal suspensions, dense microemulsions and granular materials [3].

Experimentally, Simmons *et al* [4] observed shear-thinning behaviour, where the steady-state viscosity $\eta(\dot\gamma)$ was represented by

$$\eta(\dot\gamma) = \sigma_{xy}/\dot\gamma \cong \eta(0)/(1 + \dot\gamma\tau_\eta), \tag{1}$$

in the range $7 \times 10^5 < \eta(0) < 6 \times 10^{13}$ (Poise) in soda-lime-silica glass. The characteristic time τ_η is expected to be of order τ_α. Remarkably, the shear stress σ_{xy} tends to a limiting shear stress, $\sigma_{\lim} = \eta(0)/\tau_\eta$, of order $10^{-2}\mu_0$, μ_0 being the shear modulus for infinitesimal strains.

After application of shear, they also observed an overshoot of the shear stress before approach to a steady state.

As a closely related problem, understanding of mechanical properties of amorphous metals has been of great technological importance [5, 6]. They are usually ductile in spite of their high strength. At low temperatures $T \lesssim 0.6$–$0.7T_g$, localized shear bands, where zonal slip occurs, have been observed above a yield stress. At relatively high temperatures $T \gtrsim 0.6$–$0.7T_g$, on the other hand, shear deformations are induced *homogeneously* (on macroscopic scales) throughout samples, giving rise to viscous flow with strong shear thinning behaviour. In a model amorphous metal in 3D, Maeda and Takeuchi [7] numerically followed atomic motions after application of a small shear strain to observe heterogeneities among poorly and closely packed regions. Such dynamic heterogeneities have been reported in recent simulations in sheared states [1] and also in quiescent states [8–11].

In the study of elasto-plastic dynamics of solids, microscopic simulations are informative [12–14], while mean-field theories are instructive [15, 16]. In the latter theories, the problem was reduced to that of one element obeying a stochastic process under the influence of the average stress. The aim of this paper is then to present a space–time dependent, elasto-plastic dynamical model on the basis of well defined nonlinear elastic theory. Although our theory is still preliminary, we shall see that introduction of an order parameter, representing the vacancy or the local free volume, can give rise to dramatic effects similar to those reported in [12].

2. Plastic flow in one dimension

To introduce the fundamental concepts in our problem in the simplest manner, we first present a one-dimensional model which mimics a solid with shear deformations varying only in one direction (1D slip model). We here write down the dynamic equations in the continuum representation (for simplicity). The velocity $v(x, t) = \partial u(x, t)/\partial t$ of the shear displacement $u(x, t)$ (along the y axis) is governed by

$$\rho \frac{\partial}{\partial t} v = \nabla_x [\mu_0 \gamma_0 \sin(\gamma_0^{-1} \nabla_x u)] + \eta_0 \nabla_x^2 v + \nabla_x \sigma_R, \tag{2}$$

where $\nabla_x = \partial/\partial x$, ρ is the mass density, μ_0 is the shear modulus, γ_0 is a constant determined by the underlying crystal structure and η_0 is a vicosity. The period of the strain is given by $\gamma_p = 2\pi\gamma_0$. To ensure equilibrium in the absence of applied force, we introduce the random stress $\sigma_R(x, t)$ related to η_0 via the fluctuation–dissipation relation $\langle \sigma_R(x, t)\sigma_R(x', t') \rangle = 2k_B T \eta_0 \delta(x - x')\delta(t - t')$, where T is the temperature. Hereafter space and time will be measured in units of $\ell \equiv \eta_0/(\rho\mu_0)^{1/2}$ and $\omega_0^{-1} \equiv \eta_0/\mu_0$, respectively. The dimensionless noise strength is given by $\epsilon = k_B T/\mu_0\gamma_0^2\ell$.

We numerically solve (2) on a 1D chain ($j = 0, 1, \ldots, N = 600$) with $\epsilon = 0.25$, setting $u(x, t) \to u_j(t)$ and $\partial u/\partial x \to \gamma_j \equiv u_{j+1} - u_j$. We apply a constant shear rate $\dot{\gamma}$ at $t = 0$ with $u_0 = 0$ and $u_N/\gamma_0 = N\dot{\gamma}t$. In figure 1 the average dimensionless stress $\langle \sigma \rangle(t) = N^{-1} \sum_j \sin(\gamma_j(t)/\gamma_0) + \dot{\gamma}$ is plotted as a function of the scaled strain $\dot{\gamma}t/\gamma_p$. The system undergoes a pure elastic deformation $\gamma_j(t)/\gamma_0 \cong \dot{\gamma}t$ in the initial stage, but slips (jumps of γ_j by multiples of γ_p) appear randomly throughout the system with increasing the average strain $\dot{\gamma}t$. The inset shows slips and continuously strained regions. The average slope of the latter regions gives the average stress. For the range of the shear rates in figure 1, we can see shear-thinning $\sigma_{xy} \propto \dot{\gamma}^{0.7}$ in steady states (if averaged over time).

It is also straightforward to integrate (2) under a fixed shear stress σ_{ext} applied at one end with the other end being pinned. For small σ_{ext} below a yield stress σ_y, we observe no slip
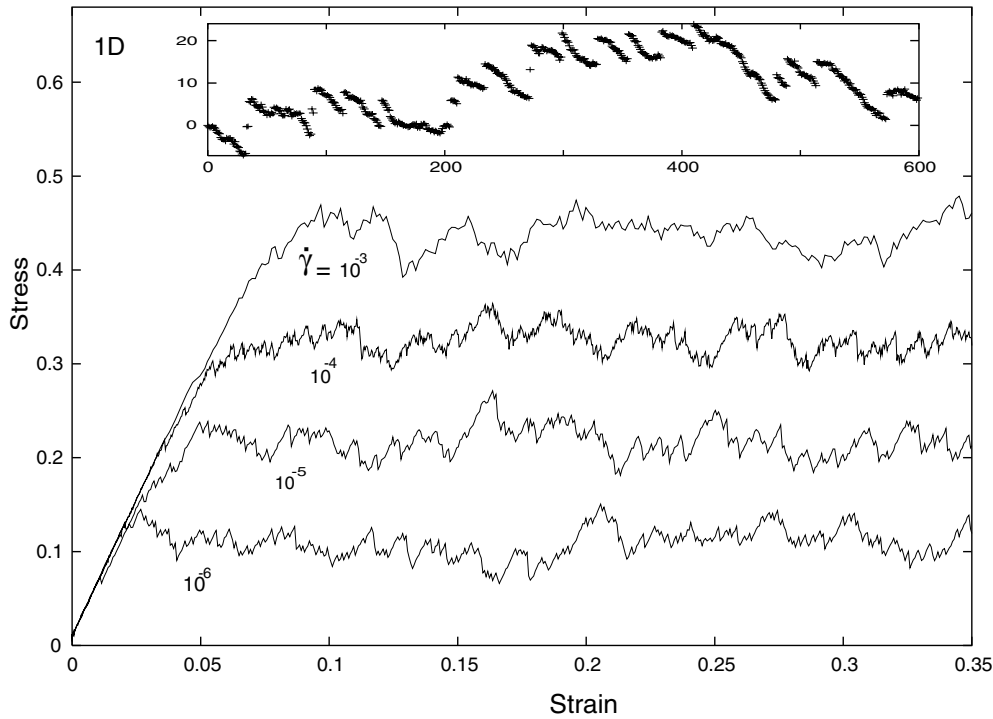
Figure 1. Stress versus strain in units of $\mu_0\gamma_0$ and γ_p obtained from the discretized version of the 1D model (1) after application of constant shear rate. Here $\dot{\gamma}/\omega_0 = 10^{-3}, 10^{-4}, 10^{-5}$ and 10^{-6} from above. The inset displays a snapshot of the deviations $u_j/\gamma_0 - \dot{\gamma}tj$ ($0 \leqslant j \leqslant 600$) at $t = 720$ for $\dot{\gamma} = 10^{-3}$.

formation, while for $\sigma_{\text{ext}} > \sigma_y$ plastic flow is produced. For the noise strength of $\epsilon = 0.25$, we find $\sigma_y \cong 0.2$.

3. Plastic flow without vacancies

As a direct generalization of (2), we set up a plastic flow model in two dimensions (2D slip model). In the continuum limit the strain components are defined by

$$e_1 = \nabla_x u_x + \nabla_y u_y, \qquad e_2 = \nabla_x u_x - \nabla_y u_y, \qquad e_3 = \nabla_x u_y + \nabla_y u_x, \quad (3)$$

where $\nabla_x = \partial/\partial x$ and $\nabla_y = \partial/\partial y$. If we suppose a triangular lattice, the elasticity is isotropic in the harmonic approximation [2], being characterized by the bulk and shear moduli, K_0 and μ_0, but it depends on the orientational angle θ of one of the crystal axes for large shear deformations. Note that, under rotation of the reference frame by θ, the shear strains e_2 and e_3 are changed to e'_2 and e'_3, where [2]

$$e'_2 = e_2 \cos 2\theta + e_3 \sin 2\theta, \qquad e'_3 = -e_2 \sin 2\theta + e_3 \cos 2\theta. \quad (4)$$

We write the elastic energy density in the form $f_{\text{el}} = K_0 e_1^2/2 + \mu_0 \mathcal{F}(e'_3, e'_2)$. The simplest form of the scaling function $\mathcal{F}$ is

$$\mathcal{F}(e'_3, e'_2) = \frac{1}{6\pi^2}\left[3 - \cos\pi\left(\sqrt{3}e'_3 - e'_2\right) - \cos\pi\left(\sqrt{3}e'_3 + e'_2\right) - \cos(2\pi e'_2)\right] \quad (5)$$
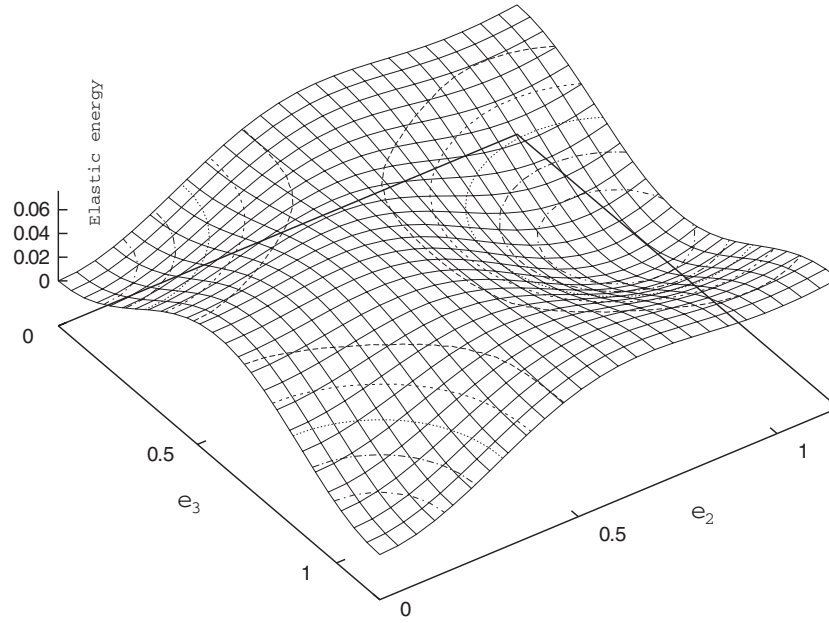
Figure 2. Function $\mathcal{F}(e_3, e_2)$ defined by (5), which represents the 2D shear deformation energy density divided by μ_0 for $\theta = 0$.

and is shown in figure 2. $\mathcal{F}$ is invariant with respect to the rotation $\theta \to \theta + \pi/3$, is a periodic function of e_3' with period $\gamma_p = 2/\sqrt{3}$ for $e_2' = 0$ (simple shear deformation) and becomes $(e_2^2 + e_3^2)/2$ for small strains. If we assume $\partial\theta/\partial t = (\nabla_x v_y - \nabla_y v_x)/2$ for the angle rotation rate, its time integration yields

$$\theta = \tfrac{1}{2}(\nabla_x u_y - \nabla_y u_x) + \theta_0, \tag{6}$$

where θ_0 is independent of t but may depend on $\boldsymbol{r} = (x, y)$. For $\theta = 0$ one of the crystal axes is along the x axis. Then the elastic energy $F_{el} = \int d\boldsymbol{r}\, f_{el}$ is a functional of $\boldsymbol{u}$. We assume that the lattice velocity $\boldsymbol{v} = \partial\boldsymbol{u}/\partial t$ obeys

$$\rho \frac{\partial}{\partial t} \boldsymbol{v} = -\frac{\delta}{\delta \boldsymbol{u}} F_{el} + \eta_0 \nabla^2 v + \nabla \cdot \overset{\leftrightarrow}{\sigma}_R, \tag{7}$$

where the first term on the right-hand side is also written as $\nabla \cdot \overset{\leftrightarrow}{\sigma}$ in term of the elastic stress tensor $\overset{\leftrightarrow}{\sigma}$. The symmetric random stress tensor $\overset{\leftrightarrow}{\sigma}_R = \{\sigma_{\alpha\beta}^R\} = \{\sigma_{\beta\alpha}^R\}$ satisfies $\sigma_{xx}^R + \sigma_{yy}^R = 0$, because the bulk viscosity is neglected in (7), and [2]

$$\langle \sigma_{\alpha\beta}^R(\boldsymbol{r}, t)\sigma_{\alpha\beta}^R(\boldsymbol{r}', t') \rangle = 2k_B T \eta_0 \delta(\boldsymbol{r} - \boldsymbol{r}')\delta(t - t'). \tag{8}$$

We measure space and time in units of $\eta_0/(\rho\mu_0)^{1/2}$ and η_0/μ_0 and the strains in units of $\gamma_p = 2/\sqrt{3}$. If these scaling units are used, the noise strength $k_B T \eta_0$ in (8) is replaced by

$$\epsilon = k_B T \rho/\gamma_p^2 \eta_0^2. \tag{9}$$

We integrate (7) on a 128×128 square lattice by applying a constant shear rate $\dot{\gamma}$ at $t = 0$ with $\epsilon = 0.1$. The periodic boundary condition is imposed in the x direction, while $\boldsymbol{u} = \boldsymbol{0}$ at the bottom $y = 0$ and $u_x = \dot{\gamma}t$ and $u_y = 0$ at the top $y = 128$. At $t = 0$, the values of $\boldsymbol{v}$ at the lattice sites are Gaussian random numbers with variance $\epsilon^{1/2}$ but $\boldsymbol{u} = \boldsymbol{0}$ and $\theta = 0.1$. In figure 3 we show the average scaled stress $\langle\sigma_{xy}\rangle/\mu_0$ as a function of the scaled strain $\dot{\gamma}t/\gamma_p$
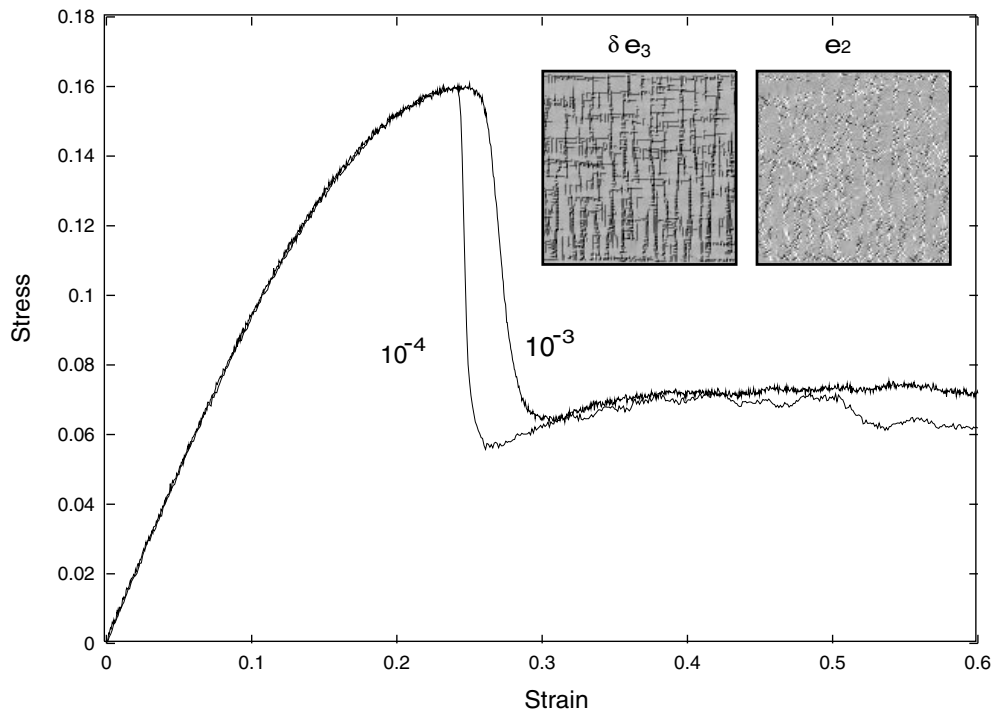
Figure 3. Stress versus strain for $\dot{\gamma} = 10^{-3}$ and 10^{-4} obtained from the 2D slip model (7). In the inset $\delta e_3 = e_3 - \gamma$ and e_2 at $t = 400$ for $\dot{\gamma} = 10^{-3}$ are shown.

for $\dot{\gamma} = 10^{-3}$ and 10^{-4}. In the inset we display snapshots of e_3 and e_2. Because we start with a perfect crystal with the initial fluctuations only in the velocity, the stress curve drops sharply after the peak with catastrophic formation of slips. Then structurally disordered states are produced where defects are proliferated (*strain-induced disordering*). Note that slips are accumulations of dislocations [17]. In the initial stage of plastic flow, we have simple slips consisting of two edge dislocations with opposite Burgers vector $\pm a$ with a being the lattice constant. The elastic energy to create such a slip is minimum in the x and y directions under shear deformation. This is the reason why the slips in figure 3 are parallel to the x or y direction. In figure 4 the shear ($=10^{-3}$) is switched off at (a) $t = 190$ before the peak time of the stress, (b) $t = 220$ just after the peak time and (c) $t = 440$. The top and bottom boundaries are kept at rest afterwards. Pure elastic deformation is maintained in (a), while no appreciable time evolution is detected after transients in (b) and (c). This means that the structurally disordered states are metastable.

4. Plastic flow with vacancies

Usually in the literature, the density deviation $\delta\rho$ is equated with $-\bar{\rho}\nabla\cdot\boldsymbol{u} = -\bar{\rho}e_1$ in solids [17], where $\bar{\rho}\,(\cong\rho)$ is the average density and $|\delta\rho| \ll \bar{\rho}$ is assumed. In the presence of vacancies or interstitials, however, there can be a small difference between these two quantities. Flemming and Cohen [18] constructed a hydrodynamic description of solids including the new variable $m \equiv \delta\rho/\bar{\rho} + e_1$. According to their theory, the *vacancy concentration* c may be defined by

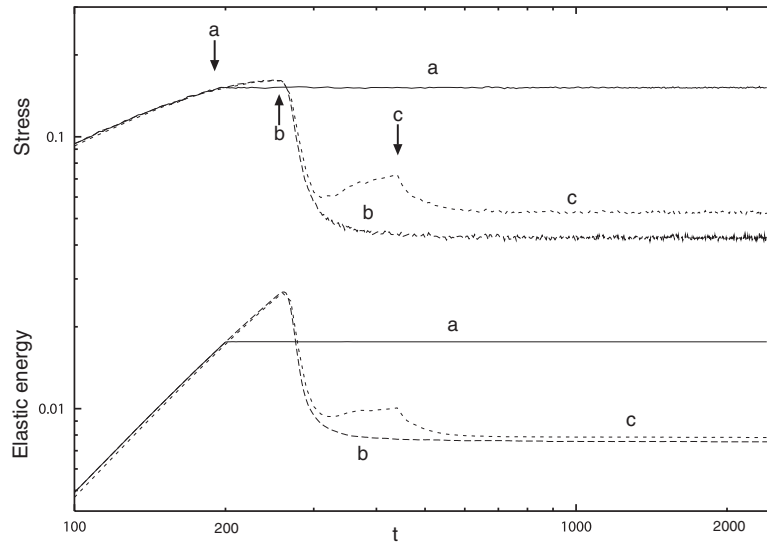$$c = c_0 - m = c_0 - (\delta\rho/\bar{\rho} + e_1) \tag{10}$$

Figure 4. Scaled stress and elastic energy versus time, which demonstrates freezing of strain-induced disordered states of (7) at long times. The shear is switched off at (a) $t = 190$, (b) $t = 220$ and (c) $t = 440$, as indicated by arrows, using the same parameters as for the curve of $\dot{\gamma} = 10^{-3}$ in figure 3.

where c_0 is the average $\langle c \rangle$ dependent on T and $\bar{\rho}$. On the other hand, Granato [19] claimed relevance of interstitials in amorphous solids because they can greatly decrease the shear modulus. However, because vacancies and interstitials are point defects, it may be more appropriate to treat c as the local free-volume fraction [18, 20] which can take continuous values at each lattice site. Then c_0 is the average free-volume fraction and we may assume $0 \leqslant c_0 \ll 1$. The role of m or c is expected to be crucial in amorphous solids. We try to include the vacancy variable in our nonlinear slip model (2D vacancy model).

The dynamic equations obeyed by the mass density and the momentum density are of the usual forms,

$$\frac{\partial}{\partial t}\delta\rho = -\bar{\rho}\nabla \cdot \boldsymbol{v}, \tag{11}$$

$$\bar{\rho}\frac{\partial}{\partial t}\boldsymbol{v} = \nabla\cdot \overset{\leftrightarrow}{\sigma} + \eta_0\nabla^2\boldsymbol{v} + \nabla\cdot \overset{\leftrightarrow}{\sigma}_{\mathrm{R}}. \tag{12}$$

In (12) the force density, the first term on the right-hand side, is written in terms of the free energy functional $F = F\{\rho, \boldsymbol{u}\}$ as

$$\nabla\cdot \overset{\leftrightarrow}{\sigma} = -\bar{\rho}\nabla(\delta F/\delta\rho)_{\boldsymbol{u}} - (\delta F/\delta\boldsymbol{u})_\rho = -(\delta F/\delta\boldsymbol{u})_m, \tag{13}$$

where use has been made of the identities $(\delta/\delta\boldsymbol{u})_\rho = (\delta/\delta\boldsymbol{u})_m - \nabla(\delta/\delta m)_{\boldsymbol{u}}$ and $(\delta/\delta m)_{\boldsymbol{u}} = \bar{\rho}(\delta/\delta\rho)_{\boldsymbol{u}}$. The random stress tensor $\overset{\leftrightarrow}{\sigma}_{\mathrm{R}}$ satisfies (8). It is important that, in the presence of the vacancy field, the lattice velocity $\partial\boldsymbol{u}/\partial t$ is different from the mass velocity $\boldsymbol{v}$ and is assumed to be of the form

$$\frac{\partial}{\partial t}\boldsymbol{u} = \boldsymbol{v} - \lambda_0\left(\frac{\delta}{\delta\boldsymbol{u}}F\right)_\rho + \zeta_{\mathrm{R}}, \tag{14}$$

where λ_0 is the kinetic coefficient and the components $\zeta_\alpha^{\mathrm{R}}$ of the random force vector ζ_{R} are characterized by

$$\langle\zeta_\alpha^{\mathrm{R}}(\boldsymbol{r}, t)\zeta_\beta^{\mathrm{R}}(\boldsymbol{r}', t')\rangle = 2k_{\mathrm{B}}T\lambda_0\delta_{\alpha\beta}\delta(\boldsymbol{r} - \boldsymbol{r}')\delta(t - t'). \tag{15}$$

From (11) and (14) the equation for m is expressed as

$$\frac{\partial}{\partial t} m = \nabla \cdot \lambda_0 \left[\nabla \left(\frac{\delta}{\delta m} F \right)_u + \nabla \cdot \overleftrightarrow{\sigma} \right] + \nabla \cdot \zeta_R. \quad (16)$$

It is worth noting that (16) is similar to the dynamic equation for the concentration in viscoelastic fluid mixtures [2, 21]. In passing, owing to the special form of (13), the time derivative of the total free energy $F\{\rho, u\} + \int dr\, \bar{\rho} v^2/2$ becomes non-negative-definite in the absence of applied stress if the random noises are neglected. This is a self-consistent condition of Langevin equations ensuring attainment of equilibrium [2].

The free energy $F = \int dr\, f$ is a functional of u and $\delta\rho$ (or m). We assume the free energy density f in the form

$$f = \frac{A}{2} m^2 + \frac{B}{4} m^4 + \alpha m e_1 + \frac{C}{2} |\nabla \delta\rho|^2 + \frac{K_0}{2} e_1^2 + \mu(m) \mathcal{F}(e_3', e_2'), \quad (17)$$

where A, B and C are positive constants and α is a coupling constant. The gradient term ($\propto C$) is introduced to suppress the density fluctuations with short length scales. (We are considering density fluctuations longer than the peak distance of the pair correlation function.) For simplicity, we neglect the other gradient terms involving the gradients of m and the strains. In our theory it is most important that the shear modulus $\mu(m)$ sensitively depends on m. Near glass transitions, with decreasing m or increasing c, $\mu(m)$ is expected to decrease abruptly from a finite value μ_0 to zero (=fluid value) around a threshold value of m or c.

Analytic calculations of the above model are difficult except for idealized situations. As a simple exercise, let us consider small deviations with wavevector k around a homogeneously strained state with $e_3 = \gamma$, where the system is at rest and the harmonic approximation can be made for the elastic energy. Then the mechanical equilibrium condition allows elimination of u from (16) [2]. We consider the steady-state variance of m in the long wavelength limit, $\chi_v = \lim_{k\to 0} \langle |m_k|^2 \rangle$, in 2D. In the linear approximation it becomes dependent on the angle of k:

$$\frac{k_B T}{\chi_v} = A - \frac{\alpha^2}{L_0} - \frac{2\alpha}{L_0} \mu_1 \gamma \sin 2\varphi - \frac{1}{L_0} (\mu_1 \gamma)^2 [1 + (\cos 2\varphi)^2 K_0/\mu_0], \quad (18)$$

where $\sin 2\varphi = 2k_x k_y/k^2$, $\mu(m) = \mu_0 + \mu_1 m + \cdots$ and $L_0 = K_0 + \mu_0$. The vacancy diffusion constant is written as $D_v = \lambda_0 k_B T/\chi_v$. The steady-state density variance $\chi_\rho = \lim_{k\to 0} \langle |\rho_k|^2 \rangle/\rho^2$ in 2D is written as

$$\chi_\rho = \frac{k_B T}{L_0} + \left[1 + \frac{1}{L_0} (\alpha + \mu_1 \gamma \sin 2\varphi) \right]^2 \chi_v. \quad (19)$$

The first term is the usual term, while the second term arises from the vacancy fluctuations. The dependence of these quantities on γ and the angle φ can become appreciable with increasing μ_1 and/or decreasing A. For $\alpha = 0$, for example, the homogeneous state is unstable for $\gamma > \gamma_c = (\mu_0 A)^{1/2}/\mu_1$ against the fluctuations with k along the x or y axis. Note that $\gamma_c \ll 1$ can hold if $\mu_1/\mu_0 \gg 1$. It is easy to confirm that essentially the same result follows in 3D in both shear and elongational deformations. Thus, in elastically deformed amorphous solids (before onset of plastic flow), we predict enhancement of the density fluctuations in particular directions of the wavevector.

We then show the numerical results of our model in (11)–(17) obtained on a 128×128 square lattice for the case of applying a constant $\dot{\gamma}$. Again the units of space, time and strains are $\eta_0/(\rho\mu_0)^{1/2}$, η_0/μ_0 and $\gamma_p = 2/\sqrt{3}$, respectively. The m is also divided by γ_p. The dimensionless mass density is given by $\delta\rho/\rho\gamma_p$. Though it is not clear what functional form of $\mu(m)$ is appropriate, we tentatively use
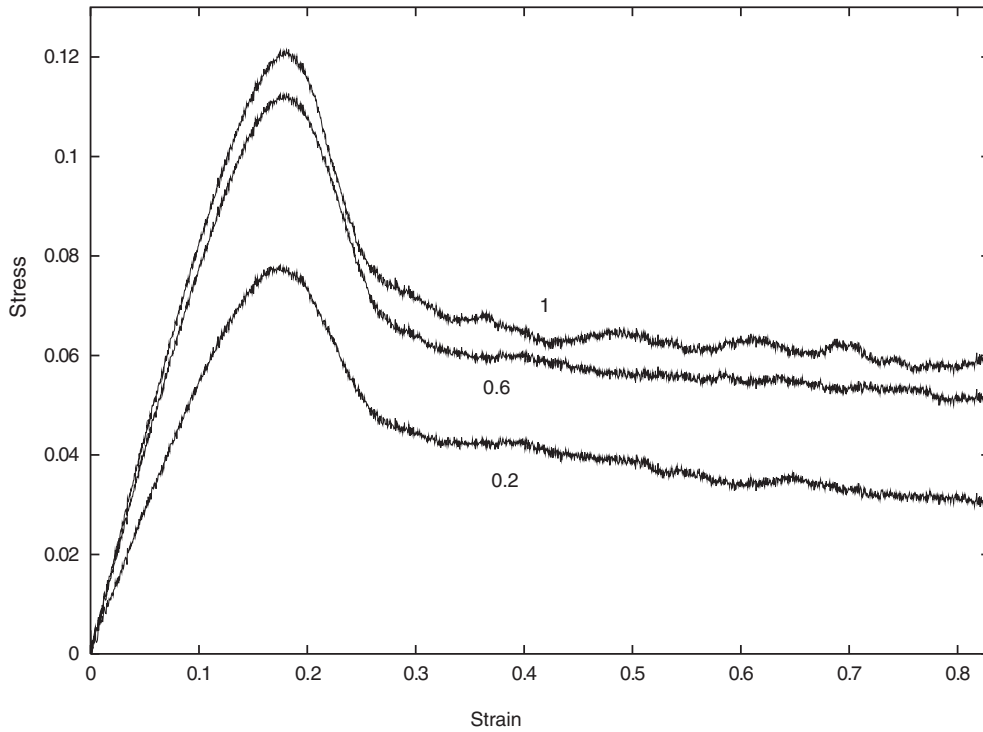
$$\mu(m) = \mu_0 \exp[-A_0/(m + m_0)] \quad (20)$$

Figure 5. Stress versus strain for $\dot{\gamma} = 10^{-3}$ obtained from integration of (11), (12) and (14) using (16) and (17) at $\dot{\gamma} = 10^{-3}$. Here $m_0 = 1$, 0.6 and 0.2 from above.

for $m+m_0 > 0$ and $\mu(m) = 0$ for $m+m_0 \leqslant 0$. Here A_0 is a constant and is set equal to 0.1 in our simulation, while m_0 is a control parameter representing the closeness to the glass transition. In fact, if $\mu(m)$ goes to zero at $c = c_c$, we have $m_0 = c_c - c_0$ from (10). However, essentially the same numerical results follow as long as $\mu(m)$ strongly depends on m (for example, from the simpler form $G(m) \propto (m + m_0)^2$ instead of (20)). The other parameter values used are $A = C = 1$, $B = 10$, $\alpha = 0$, $\lambda_0 = 0.1$ and $\epsilon = 0.1$. While the initial conditions for v, u and θ are the same as in the previous case of figures 3 and 4, we assign random Gaussian numbers with variance 0.1 to m. In figure 5 we show the time evolution of the scaled shear stress as a function of the scaled average strain $\dot{\gamma} t/\gamma_p$ at $\dot{\gamma} = 10^{-3}$ for $m_0 = 1$, 0.6 and 0.2. Figures 6(a) and (b) display snapshots of e_3, e_2, $c - c_0 = -m$ and $\delta\rho$ at $t = 250$ and 420 on the curve of $m_0 = 0.6$ in figure 5. Figure 7 demonstrates that these strain-induced disordered states are metastable as in figure 4. Salient features are as follows.

 (i) Plastic flow is induced earlier than in the absence of vacancies, because slip formation is easier in regions with smaller m. Onset of plastic flow is sensitive to the initial randomness of m.
 (ii) The effective viscosity $\eta_{\text{eff}} = \langle \sigma_{xy} \rangle / \dot{\gamma}$ becomes smaller with decreasing the parameter m_0 in (17) or increasing the elastic inhomogeneity.
(iii) The η_{eff} also decreases as a function of time on long timescales because of slow accumulation of vacancies around slips. In our model, though this tendency is considerably suppressed by the quartic term ($\propto B$) in (16), vacancy accumulation can lead to fluidization at long times after percolation of the slips.
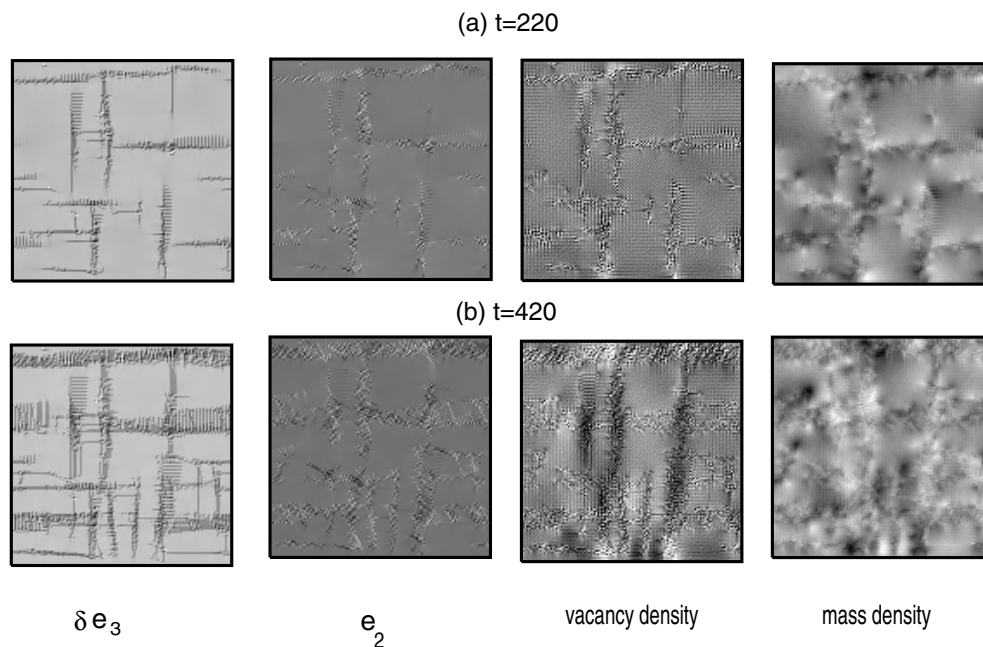(iv) The density fluctuations are induced and are frozen after cessation of shear.

(a) t=220

(b) t=420

δe_3 e_2 vacancy density   mass density

Figure 6. Snapshots of $\delta e_3 = e_3 - \gamma$, e_2, $c - c_0 = -m$ and $\delta \rho$ at (a) $t = 250$ and (b) $t = 420$ for $\dot{\gamma} = 10^{-3}$ on the curve of $m_0 = 0.6$ in figure 5.

As demonstrated in figure 7, the fluctuation variances of the vacancy and the density are much more enhanced than in the initial state. Owing to the gradient term in (16), the density smoothly varies in space (compared with m).

5. Concluding remarks

We have presented a first time-dependent Ginzburg–Landau theory accounting for inhomogeneous nonlinear elastic deformations. It is a coarse-grained theory and the sharp peak of the structure factor, which is essential in the mode coupling theory [22], does not come into play. Instead, periodicity of the elastic energy with respect to the strains e'_3 and e'_2 and vacancy dependence of the shear modulus are two major ingredients of our theory, which bring about metastable structural disordered states with heterogeneities in the vacancy and mass densities. As a closely related effect, Fischer [23] observed excess scattering from nearly static density fluctuations with sizes in a range of 20–200 nm in glass-forming fluids. We believe that such large-scale frozen fluctuations can arise only as a result of nonlinear elastic deformations induced by structural disorder. We also mention previous simulations. Argon *et al* [12] applied a tensile (elongational) strain to a 2D model to produce slips and shear bands making angles of $\pm 45°$ with respect to the stretched direction in agreement with experiments. The same results also follow from our model and will be reported shortly. We will show that the elastic energy to create a slip under tension is minimum for these directions. Ikeda *et al* [14] applied a tensile strain to a 3D model to induce a change from a perfect crystal to an amorphous solid.

However, we admit that our results are still preliminary and it remains unclear how our theory corresponds to real physical effects. In particular, the initial conditions ($\boldsymbol{u} = \boldsymbol{0}$ and $\theta = $ constant) should be inappropriate for amorphous solids (where structural disorder should
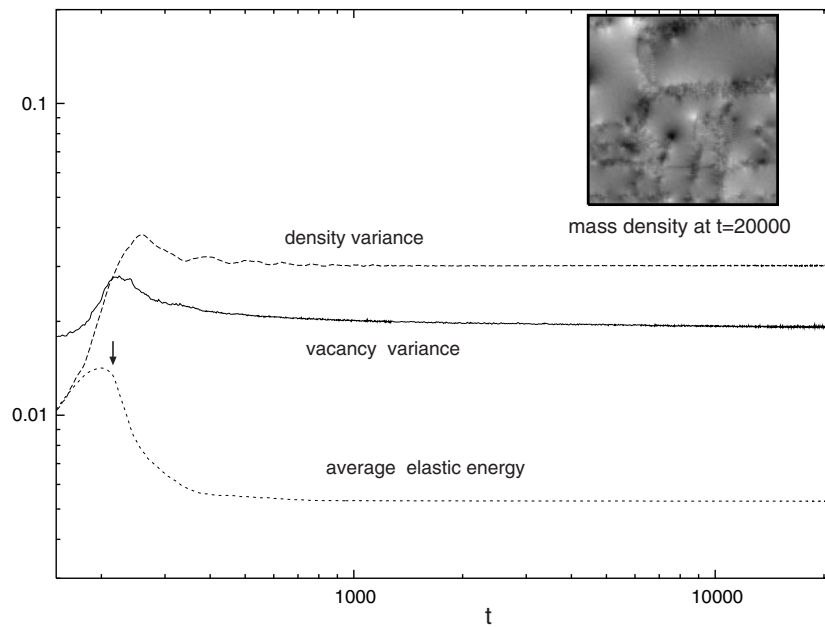
Figure 7. Freezing of strain-induced disordered states of the vacancy model. Shown are the density variance $[\langle(\delta\rho)^2\rangle]^{1/2}/\rho\gamma_p$, the vacancy variance $[\langle(\delta m)^2\rangle]^{1/2}/\gamma_p$ and the average elastic energy $\langle f_{el}\rangle$. As in figure 4, the shear rate is switched off at $t = 220$. The frozen density profile at $t = 2 \times 10^4$ is shown in the inset.

preexist even before applying strain). In future work, we should start with initial states with various amounts of disorder and should also examine what parameter values are appropriate for amorphous solids.

We mention analogous and instructive examples. In solids undergoing phase separation or structural transitions, the dependence of the shear modulus on the order parameter, written as m, in the form $\mu = \mu_0 + \mu_1 m$, is of crucial importance in phase ordering [2, 24]. In all these cases, local minimization of the nonlinear elastic energy $((\delta F/\delta u)_m = 0)$ gives rise to heterogeneous metastable states where time evolution is pinned. In viscoelastic polymer systems, the composition dependence of the viscoelastic properties can give rise to shear-induced phase separation [2, 21], where the scattered light intensity takes a form similar to χ_v in (18).

References

[1] Yamamoto R and Onuki A 1997 *Europhys. Lett.* **40** 61
    Yamamoto R and Onuki A 1998 *Phys. Rev.* E **58** 3515
[2] Onuki A 2002 *Phase Transition Dynamics* (Cambridge: Cambridge University Press)
[3] Liu A J and Nagel S R (ed) 2001 *Jamming and Rheology* (London: Taylor and Francis)
[4] Simmons J H, Mohr R K and Montrose C J 1982 *J. Appl. Phys.* **53** 4075
    Simmons J H, Ochoa R, Simmons K D and Mills J J 1988 *J. Non-Cryst. Solids* **105** 313
[5] Chen H S and Goldstein M 1971 *J. Appl. Phys.* **43** 1642
[6] Spaepen F 1977 *Acta Metall.* **25** 407
    Argon A S 1979 *Acta Metall.* **27** 47
[7] Maeda K and Takeuchi S 1981 *Phil. Mag.* A **44** 643
[8] Muranaka T and Hiwatari Y 1995 *Phys. Rev.* E **51** R2735
[9] Perera D N and Harrowell P 1996 *Phys. Rev.* E **54** 1652

[10] Yamamoto R and Onuki A 1997 *J. Phys. Soc. Japan* **66** 2545
[11] Kob W, Donati C, Plimton S J, Poole P H and Glotzer S C 1997 *Phys. Rev. Lett.* **79** 2827
[12] Mott P H, Argon A S and Suter U W 1993 *Phil. Mag.* A **67** 931
    Bulatov V V and Argon A S 1994 *Model. Simul. Mater. Sci. Eng.* **2** 167
    Bulatov V V and Argon A S 1994 *Model. Simul. Mater. Sci. Eng.* **2** 185
    Bulatov V V and Argon A S 1994 *Model. Simul. Mater. Sci. Eng.* **2** 203
[13] Falk M L and Langer J S 1998 *Phys. Rev.* E **6** 7192
[14] Ikeda H, Qi Y, Çagin T, Samwer K, Johnson W L and Goddard W A III 1999 *Phys. Rev. Lett.* **82** 2900
[15] Doi M, Harden J L and Ohta T 1993 *Macromolecules* **26** 4935
[16] Sollich P, Lequeux F, Hébrand P and Cates M 1997 *Phys. Rev. Lett.* **78** 2020
    Sollich P 1998 *Phys. Rev.* E **58** 738
[17] Landau L D and Lifshitz E M 1973 *Theory of Elasticity* (New York: Pergamon)
[18] Flemming P D III and Cohen C 1976 *Phys. Rev.* B **13** 500
    Cohen C, Flemming P D III and Gibbs J H 1976 *Phys. Rev.* B **13** 866
[19] Granato A V 1996 *J. Physique* IV **6** C8 1
[20] Turnbull D and Cohen M H 1970 *J. Chem. Phys.* **52** 3038
[21] Helfand E and Fredrickson H 1989 *Phys. Rev. Lett.* **62** 2468
[22] Bengtzelius U, Götze W and Sjölander A 1984 *J. Phys. C: Solid State Phys.* **17** 5915
    Leutheusser E 1984 *Phys. Rev.* A **29** 2765
[23] Fischer E W 1993 *Physica* A **201** 183
[24] Onuki A and Furukawa A 2001 *Phys. Rev. Lett.* **86** 452
    Onuki A 1999 *J. Phys. Soc. Japan* **68** 5